Cite this article
Marsh A, Heath A, Reddy BVV *et al.*
Scale-up effects in alkali-activated soil blocks.
Proceedings of the Institution of Civil Engineers – Construction Materials,
https://doi.org/10.1680/jcoma.19.00102

Research Article
Paper 1900102
Received 07/11/2019;
Accepted 04/08/2020

Keywords: brickwork & masonry/
developing countries/materials
technology

Construction Materials

ice Publishing

Scale-up effects in alkali-activated soil blocks

Alastair Marsh MEng, PhD
Postgraduate researcher, Department of Architecture & Civil Engineering, University of Bath, Bath, UK; Department of Civil Engineering, Indian Institute of Science, Bengaluru, India (Orcid:0000-0002-5603-4643) (corresponding author: a.marsh@bath.ac.uk)

Andrew Heath BSc, MSc, PhD, MICE, FHEA
Professor, Department of Architecture & Civil Engineering, University of Bath, Bath, UK (Orcid:0000-0003-0154-0941) (corresponding author: a.heath@bath.ac.uk)

B. V. Venkatarama Reddy BEng, MEng, PhD
Professor, Department of Civil Engineering, Indian Institute of Science, Bengaluru, India

Preethi R. Krishnamurthy MTech
Postgraduate researcher, Department of Civil Engineering, Indian Institute of Science, Bengaluru, India

Mark Evernden MEng, PhD, FHEA
Senior Lecturer, Department of Architecture & Civil Engineering, University of Bath, Bath, UK

Pascaline Patureau PhD
Research Associate, Department of Chemistry, University of Bath, Bath, UK

Pete Walker BSc, PhD, MICE, FIStructE
Professor, Department of Architecture & Civil Engineering, University of Bath, Bath, UK

Alkali activation is a novel method of soil stabilisation, which could be used for the production of compressed blocks as walling materials. Given that much of the fundamental research into the chemical behaviour of this process has been done for small specimens, there is a knowledge gap over the potential effects of increasing specimen size. In this study, blocks were made from a mix of soil, sand and sodium hydroxide solution using a manual block press. Their phase composition and microstructure were investigated using powder X-ray diffraction and scanning electron microscopy; drying behaviour and compressive strength were also measured. No major microstructural or phase differences were found between the central and edge regions of the blocks. Longer curing time had little effect on phase formation and microstructure, but resulted in increased compressive strength. There are no fundamental chemical issues obstructing the scale-up of this stabilisation method, but further research should focus on the measurement of properties in line with building standards and eliminating hazards in the manufacturing process.

1. Introduction

Earthen construction materials have been used throughout human history – they have advantages of both low cost and low environmental impact (Houben and Guillaud, 1994). In more recent history, the practice of stabilising soils to enhance their strength and durability has become more widespread – cement or lime are the most popular stabilising agents. As the embodied carbon dioxide emissions associated with Portland cement production come under greater scrutiny, there have been efforts to develop cementitious materials with lower embodied carbon dioxide (Scrivener *et al.*, 2018). One of the leading alternatives is alkali-activated materials (Provis, 2018). Alkali-activated soils are an emerging material that lies at the intersection of these two technologies: one ancient (earth construction) and one very recent (alkali activation). They have been investigated as a possible low-impact solution for producing blocks for the construction of low-rise buildings, such as housing (Diop and Grutzeck, 2008). This could help meet the construction needs of the world's growing population, especially in developing countries, while helping to prevent climate change. Their use would be very similar to how cement-stabilised soil blocks are used, albeit with the aspiration of lower embodied carbon dioxide from the use of alkali activation (Habert and Ouellet-Plamondon, 2016). There are two distinct approaches to the stabilisation of soils by alkali activation. One approach is to add a reactive aluminosilicate precursor (e.g. fly ash) to the soil – this added precursor then reacts with the alkaline activator to form a binder. The majority of previous studies have adopted this approach (Cristelo *et al.*, 2012; Narayanaswamy *et al.*, 2020; Rios *et al.*, 2016; Silva *et al.*, 2015). The other approach is to use the soil itself as the sole precursor, with the clay minerals in soil (and associated minerals, to lesser extents) reacting with the alkaline activator (Marsh *et al.*, 2019; Muñoz *et al.*, 2015). This study adopts the latter approach.

Pressed blocks are an appropriate production method for alkali-activated soils. They minimise handling of the wet mix (compared to hand-moulding methods), which is favourable given their high alkalinity at that stage of the process. The use of static compaction to produce a block of target density gives strength from the removal of voids in the soil mix, as well as a more uniform appearance and dimensions (Reddy, 2015), making these blocks more competitive with fired block specimens and concrete blocks. The manual block press is well suited for in situ production of walling blocks, especially in developing countries, due to its ease of operation and maintenance (Jagadish, 2007).

Investigation of the fundamental chemical behaviour of alkali-activated soils and clays has typically been done using small specimens, such as 18 mm × 36 mm cylinders, due to

the cost of some precursors and the small amounts of material required for characterisation (Marsh *et al.*, 2019). In contrast, the manual block press can make blocks of different sizes, but typically ranges between $305 \times 143 \times 100$ mm and $230 \times 108 \times 100$ mm (Jagadish, 2007). The scaling up of alkali-activation reactions is not a trivial aspect in the development of this technology. With respect to soil, care needs to be taken with regard to drying shrinkage when using larger individual elements in wall construction. Drying shrinkage puts limitations on the types of soil, speed of drying and potential size of individual elements used in some earth building techniques (Houben and Guillaud, 1994). With regard to alkali activation, care needs to be taken with respect to moisture transport and heating effects. Shrinkage-induced cracking can occur in clay-based geopolymer systems, depending on the aggregate content (Kuenzel *et al.*, 2014). Although rapid or flash-setting is generally only an issue in systems containing a high amount of soluble calcium (Chindaprasirt *et al.*, 2012; Lee and van Deventer, 2002), setting time is also reduced by using higher curing temperatures (Rovnaník, 2010). The dissolution and phase formation processes for both geopolymers (Granizo and Blanco, 1998; Zhang *et al.*, 2012) and zeolites (Petrova and Kirov, 1995) are exothermic. Consequently, for larger mix volumes there is the potential for reaction-generated heat to build up, reducing setting times (Wijaya and Hardjito, 2016), and potentially altering the microstructure. Unlike cement and hydraulic lime stabilisation, commonly used stabilising agents which undergo a hydration reaction, the formation of a geopolymer does not involve net consumption of water. Instead, water is a reaction medium which is temporarily consumed during the dissolution stage and released during the condensation stage (Duxson *et al.*, 2007; Weng and Sagoe-Crentsil, 2007), before removal from macro-pores and (to some extent) gel micro-pores during drying (Mastali *et al.*, 2018). Therefore, a balance is required to have enough water to facilitate the reaction, but not so much to create excessive porosity in the final microstructure (Provis *et al.*, 2010; Zuhua *et al.*, 2009). The plate-like morphology of clay particles gives them a higher demand for water than other aluminosilicate precursors such as fly ash or ground-granulated blast furnace slag (Mastali *et al.*, 2018; Provis *et al.*, 2010). This makes them less well suited for cast concrete, but more conducive to brick-making processes such as extrusion (Maskell *et al.*, 2014) or manual compaction (Diop and Grutzeck, 2008). Zeolite formation under these conditions also begins with water-mediated dissolution and then precipitation from solution (Byrappa and Adschiri, 2007). The number of water and hydroxyl groups present in the β-cage of the product phase is dependent on the exact synthesis conditions used (Engelhardt *et al.*, 1992). For both geopolymers and zeolites, the availability of sufficient water for the formation process is a key requirement. Another concern is efflorescence. This can occur in cementitious materials in general, but is a particularly acute problem in alkali-activated materials (Allahverdi *et al.*, 2015; Longhi *et al.*, 2019). These are all practical, macro-scale considerations which depend on an understanding of micro-scale processes.

The comparison between different alkali-activated systems is often difficult due to the large number of variables in composition and processing. Investigation of the effects of scaling-up in isolation is a neglected area of research, at least in the public domain. In this study, a well-characterised precursor soil – whose alkali-activation behaviour has already been characterised at small scale – has been activated at block scale using similar composition and processing conditions. The aim of this study was to investigate any variations in phase formation and microstructure between the centre and edge regions in a block, and what implications these have for its development as a viable construction material.

2. Materials and methods

2.1 Materials

The soil used is from Bengaluru, India. Its chemical and phase composition has previously been described in Marsh *et al.* (2019), but will briefly be restated here. It had a clay fraction of 36%, and kaolinite was the sole clay mineral. Other phases present were quartz, haematite, microcline and muscovite (Figure 1). The chemical composition is given in Table 1. A quartzitic river sand, known to contain no more than 5 wt% of clay, fine silt or organic impurities (Gourav and Venkatarama Reddy, 2018) in line with the standard IS:2116-1980 (BIS, 1980), was used as aggregate. The sand was sieved to <4.75 mm before use. Sodium hydroxide (NaOH) pellets

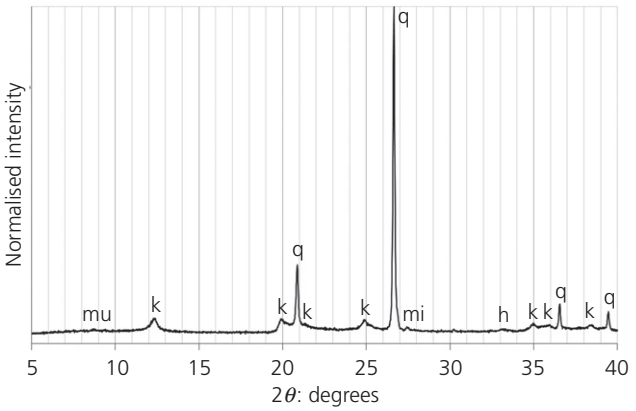

Clay minerals: k = kaolinite
Associated minerals: h = haematite, mi = microcline, mu = muscovite, q = quartz

Figure 1. Indexed X-ray diffraction (XRD) pattern of the soil precursor

Table 1. Chemical composition of the Bengaluru soil in oxide wt%

	Aluminium oxide	Calcium oxide	Copper oxide	Ferric oxide	Potassium oxide	Magnesium oxide	Silicon dioxide	Sulfur trioxide	Titanium dioxide	Total
Bengaluru soil	24.05	0.38	0.08	12.10	1.21	0.26	60.73	0.08	1.11	100.00

(>97.5% purity, Thomas Baker) were mixed with water to make a 12 M sodium hydroxide solution.

2.2 Manufacturing procedure

A 50% aggregate mix was chosen in order to reduce the overall clay content in the mix to 18%, within the recommended range of clay content for cement-stabilised soil blocks (Walker and Stace, 1997). At higher clay contents, the clay clumps together and does not mix well at this scale. The mix quantities are given in Table 2. For the quantity and concentration of sodium hydroxide solution, and assuming kaolinite to be the only reactive aluminium-containing phase in the soil, this gave a molar ratio of sodium:aluminium (Na:Al) = 0.86.

The water mass values used here are proportionally lower to the mass of dry components than those used in the manufacture of smaller samples. This is partly due to the use of 50% aggregate, but also due to the difference between the extrusion and static compaction processing methods. For extrusion, the soil is required to have plastic consistency in order to achieve flow; but for static compaction, it is better for the soil to have a more friable consistency. For the manual block press using static compaction, it is desirable for the soil to have the optimum moisture content for this compaction method in order to achieve maximum dry density under the given compaction force.

The steps in the block specimen manufacture process are shown in Figure 2. The sodium hydroxide solution was mixed and left covered, to dissolve and cool overnight. The soil and sand were added together as a 40 kg batch in a 90 kg capacity pan-mixer and dry-mixed at a speed of 27 r/min for 2 min. The water or sodium hydroxide solution was slowly added, and then wet-mixed for a further 3 min (Figure 2(a)). Any residual lumps were broken up by hand (Figure 2(b)), and the mixture was covered with sacks to reduce drying out. A reverse toggle manual block press developed by the Department of Civil Engineering at the Indian Institute of Science was used (Reddy, 2015) to produce block specimens of dimensions $230 \times 110 \times 70$ mm (Figures 2(d)–2(f)). A fixed mass of 3.64 kg of wet mix was used for each block specimen (Figure 2(c)) to achieve a target density of 1.83 g/cm^3 under static compaction, which is within the recommended range of 1.80–1.85 g/cm^3 (Jagadish, 2007).

Table 2. Mix proportions for control and activated block specimens

Mix parameter	Control	Activated
Soil mass: kg	20.00	20.00
Sand mass: kg	20.00	20.00
Water mass: kg	4.00	3.59
Sodium hydroxide dry mass: kg	0	1.92
Solution molarity: M	n/a	12

Once pressed, the block specimens were placed into an 80°C oven, and cured for either 24 h or 120 h. One activated block specimen was not oven cured, for comparison. The naming conventions for each sample are given in Table 3. After heat curing, the specimens were left to age indoors in atmospheric conditions, with all doors to the room left open during the daytime for a high air change rate. In the ageing period, average outdoor temperature was 22.6°C (ranging from 19.6°C to 27.6°C) and average outdoor relative humidity was 82% (ranging from 59% to 98%). Data were collected from Bengaluru weather station (USAF #432950) (NCEI, 2018).

2.3 Characterisation and measurements

To compare behaviour in the centre and edge of the block specimens, material was obtained from the central 50 mm region as well as the 5 mm border at the edge of the block specimens. To prepare powder for characterisation, the material was dry-ground in a ceramic pestle and mortar, and sieved through a 300 μm sieve, to remove the large sand aggregate particles.

Powder XRD patterns were taken with a Bruker D8 Advance diffractometer using copper (Cu) Kα ($\lambda = 1.54060$ Å) X-radiation using a step size of 0.02° (2θ). For the precursor soil and act-120 h samples, a different Bruker D8 Advance diffractometer was used with monochromatic Cu Kα ($\lambda = 1.540598$ Å) X-radiation and a step size of 0.016° (2θ). Patterns were corrected for specimen height shift by calibrating to the most intense quartz reflection (101) at 26.6° (2θ), and normalised to the most intense reflection in each respective pattern. Phase identification was done using Bruker EVA software.

Scanning electron microscope (SEM) imaging was used to characterise phase size and morphology, using a Jeol SEM6480LV in secondary electron mode with an accelerating

Figure 2. Stages in block specimen manufacture: (a) mixing the soil, sand and activating solution; (b) breaking up any remnant lumps in the wet mix; (c) weighing out a set amount of wet mix for each block specimen; (d) filling the mould with the wet mix; (e) compacting the block specimen; (f) releasing the block specimen from the mould

voltage (AV) of 10 kV. Bulk specimens were sputter coated with gold for 3 min.

Unconfined compressive strength (UCS) testing was done at 7 ± 1 days ageing time, using a TUN600 universal testing machine. At least four block specimens were tested for each series. The frogs on both sides of each block specimen were filled in with a mix of plaster of Paris and <1.18 mm sieved sand to create a level surface.

The mass change behaviour of the block specimens was measured after curing, and after 7 days' ageing time. The average values and standard deviations were calculated for ≥4 measurements for each series. Moisture content was measured

Table 3. Details for each sample and its abbreviation

Sample abbreviation	Control or activated	Curing time: h	Location in block
Cont-24h-e	Control	24	Edge
Cont-24h-c	Control	24	Centre
Act-24h-e	Activated	24	Edge
Act-24h-c	Activated	24	Centre
Act-120h-e	Activated	120	Edge
Act-120h-c	Activated	120	Centre
Act-0h-e	Activated	0	Edge

at 7 days ageing by removing a 60–80 g piece of material from the centre of a block specimen, and measuring the mass change after ≥24 hours drying at ≥80°C. Bulk density values were calculated from mass and volume measurements on at least four block specimens under atmospheric conditions, also at 7 days ageing. Dry density values were calculated by subtracting moisture mass (provided by the measured moisture content) from the block masses measured under atmospheric conditions.

3. Results

3.1 X-ray diffraction

The XRD patterns comparing the cont-24h, act-24h and act-120h specimens are given in Figure 3. In the control specimens, the phases present were kaolinite, albite, quartz, muscovite and microcline. For simplicity of viewing, where associated minerals (i.e. quartz, albite, muscovite and microcline) have been indexed in the control specimen patterns, these have not been indexed again in the activated specimen patterns. There was some variation in the intensity of the 002 microcline reflection at 27.5° 2θ between patterns – however, there was no consistent difference between the control and activated samples. This variation has been previously observed in alkali-activated soil systems (Marsh *et al*., 2019), and is likely to be due to orientation effects.

In all of the act-24h and act-120h block specimens, a hydrosodalite phase was formed. This is a known transformation from kaolinite under these processing conditions (Marsh *et al*., 2018). The kaolinite was not fully consumed in any of the activated block specimens, as evidenced by the residual kaolinite peaks. The peak profiles of all the hydrosodalite reflections were broad, suggesting the crystallites were small and/or highly strained (Burton *et al*., 2009). There were small differences in the peak positions of the 310 (32.6–32.9° 2θ) and 222 (34.9–35.1° 2θ) reflections between the act-24h and act-120h specimens. This is likely to mean that the cage contents of the hydrosodalite phases were slightly different, with different amounts of water and/or hydroxyl groups in the β-cage (Engelhardt *et al*., 1992). The peaks were too broad to conclusively assign a specific hydrosodalite phase. Overall, no large differences were observed between the patterns from the centre and edge regions in any of these block specimens.

XRD patterns from the edge regions of the cont-24h, act-0h and act-24h blocks are compared in Figure 4. Also included is a pattern from some of the surface efflorescence collected from the act-0h block specimen after 5 days ageing, as shown later in Figure 9. No hydrosodalite was formed in the act-0h block

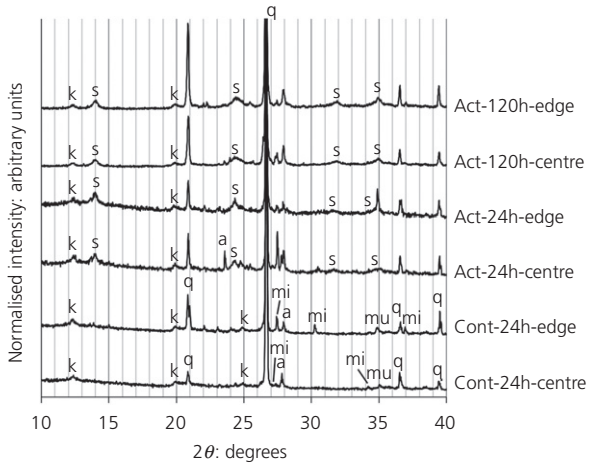

Precursor phases: a = albite; k = kaolinite; mi = microcline; mu = muscovite; q = quartz
Product phases: s = sodalite

Figure 3. XRD patterns of the centre and edge regions of cont-24h, act-24h and act-120h block specimens

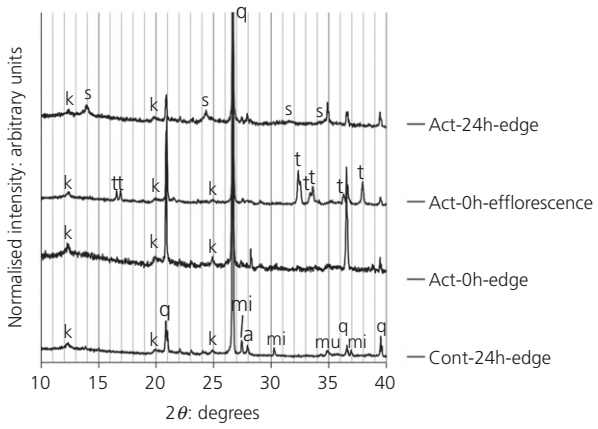

Precursor phases: a = albite; k = kaolinite; mi = microcline; mu = muscovite; q = quartz
Product phases: s = sodalite, t = thermonatrite

Figure 4. XRD patterns showing different behaviour in the edge region of the block specimens for different levels of activation and curing time

specimen. The efflorescence was composed of thermonatrite ($Na_2CO_3 \cdot H_2O$), one of several possible efflorescence phases in alkali-activated materials (Allahverdi *et al.*, 2015), along with other phases from the act-0h block specimen. The thermonatrite is likely to have been formed by atmospheric carbonation of residual sodium hydroxide in the presence of water.

3.2 Secondary electron microscopy

The SEM images of the centre and edge regions of the cont-24h, act-24h and act-120h block specimens are given for low (Figure 5) and high (Figure 6) magnifications. At low magnification (Figure 5), the large quartz aggregate particles were visible in some of the images, with particles from the finer soil fraction in between. Fine-scale cracking between the large quartz aggregate particles and the soil was observed in the activated block specimens, but not in the control block specimen. This is consistent with observations of drying-induced micro-cracking in alkali-activated metakaolin–sand mixes (Kuenzel *et al.*, 2014). At high magnification (Figure 6), the microstructural features were consistently fine, typically <1 μm, but also with some very fine particles <200 nm. In the control specimens, out of the phases known to be present from the XRD analysis, kaolinite, haematite and possibly quartz are known to be present at these size scales (Dixon and Weed, 1989). In the activated specimens, it is known from the XRD analysis that the same phases are still there, in addition to hydrosodalite. As described in Section 3.1, hydrosodalite could be expected to be present at a very fine scale. Comparing the scale of microstructural features at high magnification in the block specimens, there were no significant differences between the control and activated specimens, the 24 and 120 h cured specimens, nor between the centre and edge regions.

3.3 Drying behaviour

The changes in mass of the control and activated block specimens with ageing time are given in Figure 7. Within the 24 h cured block specimens, there was a clear difference between the control and activated block specimens. The control blocks continuously decreased in mass up to 7 days' ageing, whereas the activated block specimens maintained an approximately constant mass. This could have been be due to: (*a*) the formation of a surface barrier preventing moisture loss; (*b*) atmospheric reactions that resulted in mass gain which offset any mass loss from drying; or (*c*) re-adsorption of

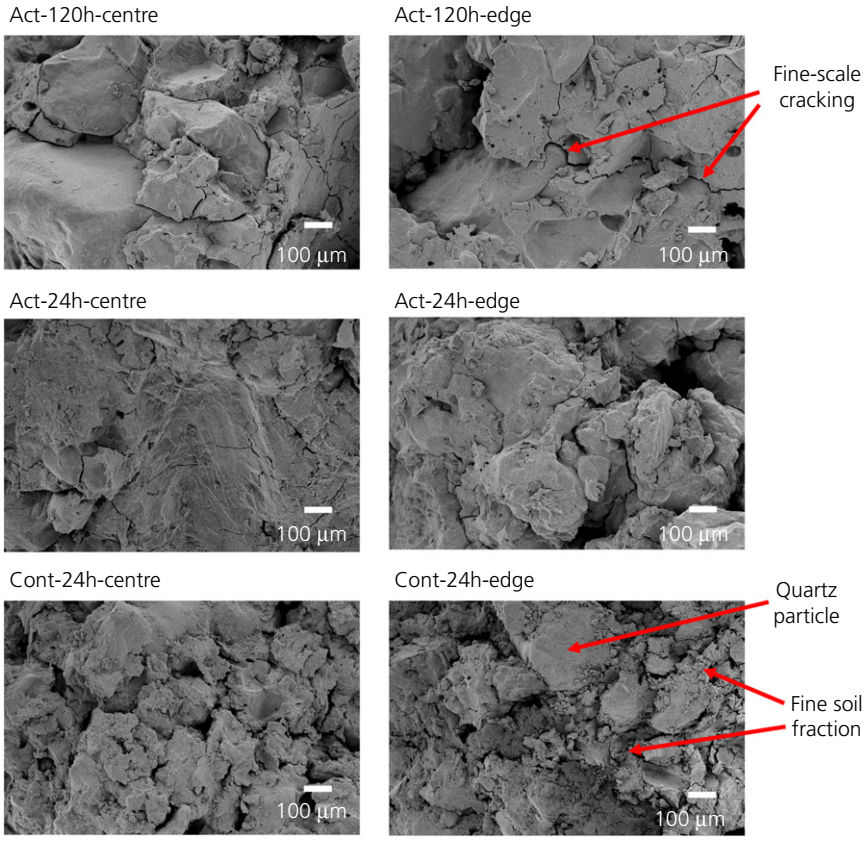

Figure 5. SEM images of centre and edge regions of cont-24h, act-24h and act-120h block specimens at 100× magnification

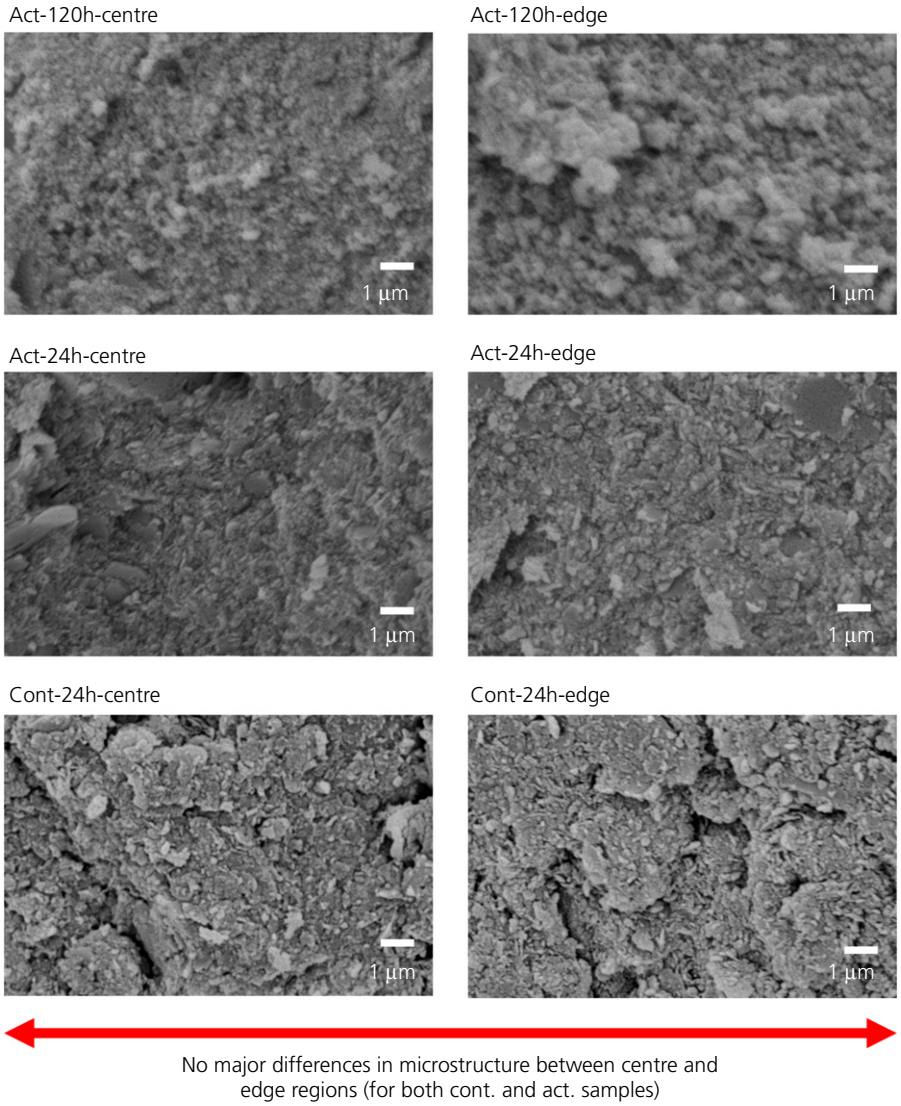

Figure 6. SEM images of centre and edge regions of cont-24h, act-24h and act-120h block specimens at 10 000× magnification

moisture from the atmosphere. No chemical hydration reactions were expected, given the chemical and phase composition of the precursors. Within the 120 h cured block specimens, both the control and activated block specimens underwent a small increase in mass. This suggests that during the longer curing time, all excess moisture from mixing was driven off, and on return to atmospheric conditions the blocks underwent moisture re-adsorption (McGregor *et al*., 2014).

Immediately after demoulding, the control and activated block specimens looked nearly identical in appearance, as shown in Figure 8. With increasing ageing time, the act-0h block specimen formed a profusion of white efflorescence, as shown in Figure 9, forming needle-like crystals. This was extreme, but some minor efflorescence was also observed for some of the act-24h block specimens by 4 days of ageing.

3.4 Unconfined compressive strength

Air-dry UCS results for control and activated block specimens at 24 and 120 h curing times are shown in Figure 10. Both control block specimens had low strength of <1 MPa. The act-24h block specimens had a slightly higher average strength than the cont-24h blocks, but this was smaller than the standard error. In contrast, the act-120h block specimens had a far higher average strength of 10.7 MPa. All block specimens

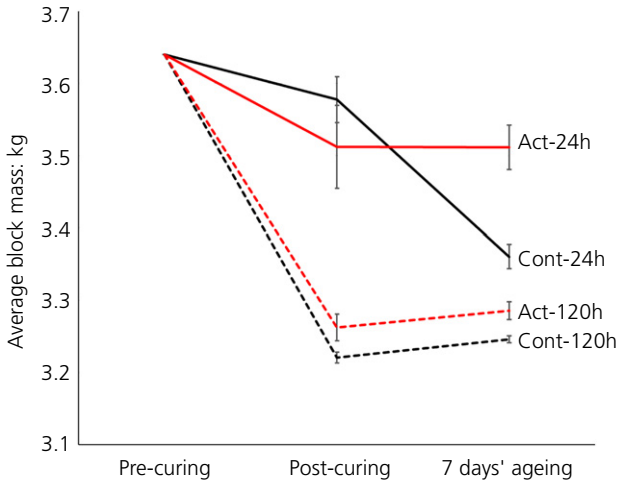

Figure 7. Changes in block specimen mass at different stages in the ageing process

Figure 8. Comparison of the control (a) and activated (b) block specimens immediately after compaction and demoulding

failed with the 'hourglass' failure pattern, which is a valid mode of failure in compression (BSI, 2009).

Values for moisture content, bulk density and dry density for the block specimens at testing are given in Table 4. The moisture content at testing for the activated block specimens was higher than for the control block specimens, and the dry density was lower for the activated block specimens. Act-120h, which had by far the highest failure strength, also had the lowest dry density of all the block series tested. This indicated that the reason for the greater strength was not a smaller void proportion.

4. Discussion

4.1 Microstructure and properties

As described in Sections 3.1 and 3.2, there were no large differences in phase composition or microstructure between the centre and edge regions. Any differences in the exact phase and size of the hydrosodalite reaction products are unlikely to result in any large differences in performance as a walling material. It is also noted that the microstructures and phase

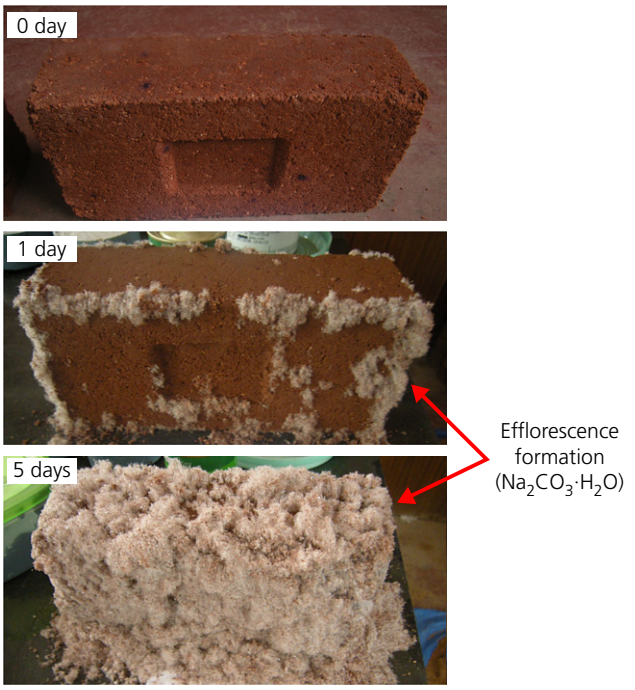

Figure 9. The act-0h block specimen after demoulding (0 days), and after 1 and 5 days of ageing

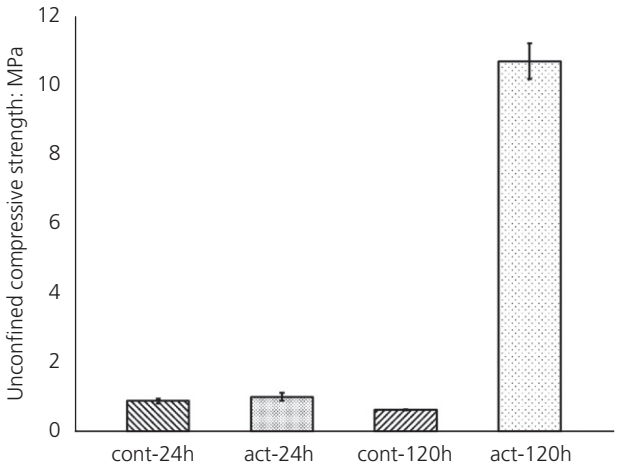

Figure 10. Air-dry UCS results for control and activated block specimens at 24 and 120 h curing times

formation of the activated block specimens were very similar to that of a small block specimen made without aggregate, as described by Marsh *et al.* (2019). This suggests that the addition of inert aggregate, use of a larger mould size and lower moisture content did not result in any fundamental changes in the alkali-activation process.

Table 4. Moisture content, bulk density, calculated dry density and average dimensions for the block specimens at 7 days ageing

	Cont-24h	Act-24h	Cont-120h	Act-120h
Moisture content: %	3.6	9.5	2.1	4.1
Bulk density: g/cm^3	1.96	1.99	1.86	1.83
Dry density: g/cm^3	1.89	1.80	1.82	1.75
Average dimensions: mm	227.0 × 108.3 × 69.8	229.8 × 109.0 × 70.5	228.4 × 108.8 × 70.2	230.0 × 109.8 × 71.0

Regarding the effects of curing time, the mass change results (Section 3.3) show that 24 h was not sufficient for the control block specimen to fully dry. This was consistent with the curing of small 18 × 36 mm cylinders of the same soil in Marsh *et al*. (2019). Although 24 h was sufficient to cause an alkali-activation reaction in the act-24h block specimens, the strength results described in Section 3.4 show that this did not result in a meaningful increase in strength. In contrast, the act-120h block specimens demonstrated a large increase in strength compared to cont-120h. This was despite the fact that the phase formation behaviour and microstructure were very similar for the act-24h and act-120h blocks, but this may be influenced by other larger-scale factors. In cement-stabilised soil block specimens, it has been shown that compressive strength increases linearly with cement content, and that strength is higher when clay content is lower (Walker and Stace, 1997). However, the XRD results show that there is unreacted kaolinite in both the act-24h and act-120h block specimens, and their peak intensities suggest there was not a large difference in the extent of reaction between the two. The lower moisture content at testing (also given in Section 3.4) for act-120h compared to act-24h could explain some of the strength difference (Champiré *et al*., 2016), but may not fully explain such a large difference in behaviour. Other factors which can influence mechanical behaviour in alkali-activated and soil systems include: particle grading, compacted density and the binding between the different phases. Although finely grained soils have been shown to have a lower void ratio and hence higher strength than coarse-grained soils in cement-stabilised soil block specimens (Reddy and Latha, 2014), the same soil and sand was used in all block specimens tested.

Regarding compacted density, the act-120h block specimens had the lowest calculated dry density of all the samples tested (Section 3.4), and it was hypothesised that this could be due to the hydrosodalite phase having a lower particle density than the original kaolinite. Additional experimentation was therefore undertaken to investigate the influence of the kaolinite to hydrosodalite phase transformation on density. Because it was difficult to extract the kaolinite mineral from the soil, high-purity Imerys Speswhite kaolin was used for this additional experimentation, activated with sodium hydroxide solutions made with sodium hydroxide pellets of >98% purity (Sigma-Aldrich, product #06203). Particle density was measured by helium (He) gas displacement using a Micromeritics Accupyc 1330. Before measurement, powder samples were degassed at 150°C under vacuum for 1 h.

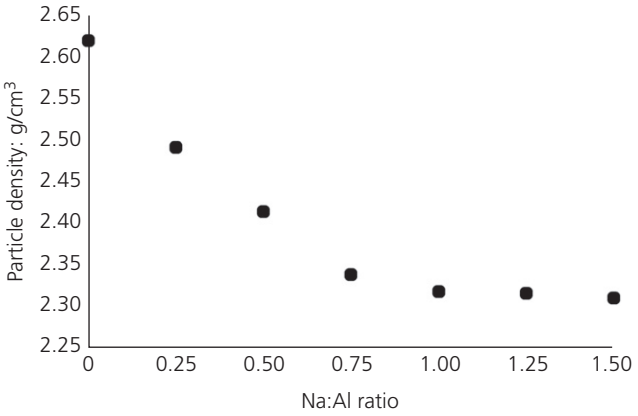

Figure 11. The variation of particle density with Na:Al ratio in an alkali-activated kaolinite system

The particle density for a kaolinite precursor was 2.62 g/cm^3, which decreased to 2.32 g/cm^3 after alkali activation at Na:Al = 1 (an 11% reduction) (Figure 11). In this system, it is known that a significant proportion of the kaolinite is transformed into hydrosodalite (Marsh *et al*., 2018), and the measured particle density value agrees well with the theoretical value for hydrosodalite calculated from a structural model (Kendrick and Dann, 2004). The lower density of hydrosodalite arises from its cage-like structure, which forms interconnected pores of approximately 12 nm in size (Franus *et al*., 2014). Given that kaolinite comprised 16.3 wt% of the wet mix, and the transformation is associated with an 11% reduction in particle density, one would expect a bulk density reduction of approximately 1.9% in the activated block specimens (approximating that all kaolinite was transformed to hydrosodalite), compared to the control specimens. This value of 1.9% reduction is less than the bulk density reductions observed between the activated and control samples (3.8–4.8%). A comparison of the sample dimensions (Table 4) showed that the control samples shrunk 2.9% (24 h curing) and 2.7% (120 h curing) relative to the activated samples. This was most likely due to drying shrinkage of the unstabilised control samples (Walker, 1995), which led to an increase in dry

density as the volume decreased. This indicates that not only does the conversion of kaolin to hydrosodalite result in a decreased particle density, but it can also reduce the amount of drying shrinkage.

Now that some explanation of the changes in density has been given, the question still remains of what other factors could contribute to the large difference in strength between the act-120h and act-24h block specimens. Differences in interaction strength between the different phases at an atomic scale could also make a contribution. For a sodium silicate–quartz system, it has been shown that the curing temperature has an effect on the bonding mechanism between the sodium silicate phase and quartz particles, which then has a large effect on strength (Lucas *et al.*, 2011). Although the chemistry is different, it is a precedent which suggests that curing conditions could influence interaction between aggregate particles and a binder phase. In summary, the difference in strength between the act-24h and act-120h specimens is likely to be due to some combination of the effects of moisture content at testing, and the chemical and/or mechanical interaction between the product phase and aggregate. The size, morphology and crystallinity degree of the particles could have a minor effect as well.

Regarding the effects of ageing time, the most notable observation was the difference in mass change between the cont-24h and act-24 h specimens (Figure 7). Of the possible explanations for this difference, the existence of a surface barrier preventing moisture loss seems unlikely. The act-120h block specimens continued to lose more moisture during a longer curing time, so a preventative barrier could not have formed within the first 24 h. For reactions that would increase mass, some minor efflorescence (thermonatrite) had formed on the act-24h specimens by 4 days of ageing, as stated in Sections 3.1 and 3.3. Since the formation of thermonatrite consumes atmospheric carbon dioxide, it would increase the mass of the specimen. However, it is not straightforward to determine the size of this contribution to the observed mass gain of act-24h with ageing. As the act-0h-e XRD pattern in Figure 4 shows, even when thermonatrite dominates the specimen, its XRD peaks are not the dominant peaks. Therefore, moderate amounts of thermonatrite could be present in the act-24h specimen, but be undetected by XRD. The remaining possible explanation for this mass increase is the re-adsorption of moisture from the atmosphere. Alkali-activated soils have been shown to have an increased capacity for moisture adsorption ($\leq$+2%) in the relative humidity range of 60–90% – that is, the capillary condensation domain (McGregor *et al.*, 2014). This agrees well with thermogravimetric measurements in simple hydrosodalite–kaolinite systems, which give a similar value of +2% for the difference in surface-adsorbed moisture mass in hydrosodalite compared to kaolinite (Marsh *et al.*, 2018). Given this, the re-adsorption rate of act-24h would be expected to be higher than that of cont-24h. It is therefore likely that the observed mass change is due to a combination of moisture re-adsorption and some carbonation. This has consequence for these materials' performance as walling materials, as hygroscopic behaviour influences both strength and moisture buffering of the indoor environment (McGregor *et al.*, 2016).

4.2 Implications for practical adoption

The strength values for the act-120h block specimens are promising, as they demonstrated a large increase over the cont-120 h block specimens. These would fulfil the strength requirements of 2.9 MPa for autoclaved aerated concrete (AAC) masonry blocks – this is a suitable comparison material for how earth materials could be used in construction (Heath *et al.*, 2012) – tested at 6% moisture content, under part A of the UK Building Regulations (HM Government, 2013). There is some debate about what constitutes appropriate testing conditions, given that these should represent service conditions (Morel *et al.*, 2007). However, if such materials are to compete with fired bricks and concrete blocks in load-bearing walling, then saturated strength testing would be essential for any alkali-activated soil blocks before use in construction. The Indian standard for stabilized soil blocks (IS 1725 : 2013) (BIS, 2013) demands a saturated compressive strength of $\geq$3.5 MPa, using the same testing procedure as used for fired clay bricks (IS 3495-1 : 1992) (BIS, 1992). More widely, it is recommended that a saturated compressive strength of 3–4 MPa is required for two-storey construction, while 2.5–3 MPa is acceptable for single-storey construction or non-load-bearing walls (Jagadish, 2007). Now that the phase formation behaviour of these blocks has been established, further testing on blocks with an optimised activating solution would show whether they could meet the saturated strength requirements.

For hydrosodalite stabilisation, an increase in strength is accompanied by a decrease in density, as shown in the preceding section. This is the opposite trend observed for cement stabilisation (Reddy and Latha, 2014). While dry density is determined by compaction force and moulding moisture content (Reeves *et al.*, 2006), in some circumstances a measurement of density change could be used to verify that the reaction has occurred. Regarding the influence on other engineering properties aside from strength, a decrease in bulk density is associated with an increase in thermal conductivity for earthen materials (Walker *et al.*, 2005). However, the scale of the decrease observed here would be unlikely to result in a significant change in thermal performance.

The soil used in this study contained kaolinite as the sole clay mineral. Different clay minerals respond in different ways to alkali activation, both in terms of reactivity and phase

formation (Khalifa *et al.*, 2020); therefore, further work is required to establish how transferrable these observations are to soils with substantially different clay mineralogy. For example, black cotton soils are widespread in India, and exhibit swelling behaviour due to the presence of expansive montmorillonite clay minerals (Sivapullaiah *et al.*, 2000). For these soils to be used for block making, it would need to be established whether the alkali-activation process could sufficiently reduce their swelling capacity: either by consumption of the montmorillonite and/or altering its interlayer chemistry.

Another practical issue is the specific hazards of alkali activation in the construction process. The use of highly alkaline substances such as 12 M sodium hydroxide solution is routine in laboratory settings. This is safe, given the right precautions and protective measures. However, in many areas of the world where population growth and demand for housing is highest, protective measures on construction sites are often the poorest. For the 40 kg soil–sand mix used in this study, direct handling of 4 l of 12 M sodium hydroxide solution was required. While other properties of a given soil mix, such as environmental impacts, depend on the exact amounts of solution used, in terms of health and safety, any exposure to such highly alkaline substances is a hazard (Narayanaswamy *et al.*, 2020). There have been efforts to find less hazardous substances in industry, but in publicly available research, this is still a relatively neglected topic (Heath *et al.*, 2014).

5. Conclusions

In this investigation of the variation within alkali-activated soil block specimens, it was found that there were no major differences in phase formation or microstructure between the central and edge regions of the block specimens. Alkali activation resulted in a large increase in compressive strength after 120 h of curing, but not after 24 h. Although the addition of inert aggregate has been shown not to affect the fundamental reactions occurring in alkali activation, it could yet be the case that the interaction between the stabilising phase (in this system, a hydrosodalite) and the aggregate is an influential parameter on overall mechanical behaviour. There are no fundamental barriers in system chemistry that prevent the use of alkali activation to produce compressed soil blocks for walling. In order to make these materials viable for industrial production, improvement is required for both the mix design and the production process – this is in order to maximise strength, prevent efflorescence and eliminate hazards to workers.

Acknowledgements

The authors acknowledge the Masonry Laboratory, Department of Civil Engineering, for hosting A. Marsh on a research placement at the Indian Institute of Science. The authors thank Mr Nikhil Venugopal, Mr Nikhilash and Mr Raghu for assistance with block specimen production, and Mr Fosas De Pando for assistance with obtaining weather data. This document is an output from the UKIERI (UK India Education and Research Initiative) project (UGC 2016-17-063) funded by the UK Department for Business, Energy and Industrial Strategy (BEIS), Foreign and Commonwealth office (FCO), British Council Division, Indian Ministry of Human Resource Development, Department of Science and Technology, Ministry of Skills Development and Entrepreneurship, The Scottish Government, Department of Economy-Northern Ireland and Welsh Government for the benefit of the Indian and UK Higher and Further Education Sector. The views expressed are not necessarily those of the funding bodies. This study was also supported by the EPSRC Centre for Decarbonisation of the Built Environment (dCarb) (grant number EP/L016869/1) and a University of Bath Research Scholarship. All data created during this research are openly available from the University of Bath data archive at https://doi.org/10.15125/BATH-00564.

REFERENCES

Allahverdi A, Najafi Kani E, Hossain KMA and Lachemi M (2015) 17 – Methods to control efflorescence in alkali-activated cement-based materials. In *Handbook of Alkali-Activated Cements, Mortars and Concretes* (Pacheco-Torgal F, Labrincha J, Leonelli C, Palomo A and Chindaprasirt P (eds)). Woodhead Publishing, Oxford, UK, pp. 463–483.

BIS (1980) IS:2116-1980 Specification for Sand for Masonry Mortars. Bureau of Indian Standards, New Delhi, India.

BIS (1992) IS 3495-1 : 1992. Methods of Tests of Burnt Clay Building Bricks. Part 1. Determination of Compressive Strength. Bureau of Indian Standards, New Delhi, India.

BIS (2013) IS 1725 : 2013. Stabilized Soil Blocks Used in General Building Construction – Specification. Bureau of Indian Standards, New Delhi, India.

BSI (2009) BS EN12390-3 : 2009. Testing Hardened Concrete. Part 3: Compressive Strength of Test Specimens. BSI, London, UK.

Burton AW, Ong K, Rea T and Chan IY (2009) On the estimation of average crystallite size of zeolites from the Scherrer equation: a critical evaluation of its application to zeolites with one-dimensional pore systems. *Microporous and Mesoporous Materials* **117(1)**: 75–90.

Byrappa K and Adschiri T (2007) Hydrothermal technology for nanotechnology. *Progress in Crystal Growth and Characterization of Materials* **53(2)**: 117–166.

Champiré F, Fabbri A, Morel JC, Wong H and McGregor F (2016) Impact of relative humidity on the mechanical behavior of compacted earth as a building material. *Construction and Building Materials* **110**: 70–78.

Chindaprasirt P, De Silva P, Sagoe-Crentsil K and Hanjitsuwan S (2012) Effect of SiO_2 and Al_2O_3 on the setting and hardening of high calcium fly ash-based geopolymer systems. *Journal of Materials Science* **47(12)**: 4876–4883.

Cristelo N, Glendinning S, Fernandes L and Pinto AT (2012) Effect of calcium content on soil stabilisation with alkaline activation. *Construction and Building Materials* **29**: 167–174.

Diop MB and Grutzeck MW (2008) Low temperature process to create brick. *Construction and Building Materials* **22(6)**: 1114–1121.

Dixon JB and Weed SB (1989) *Minerals in Soil Environments*, 2nd edn. Soil Science Society of America, Madison, WI, USA.

Duxson P, Fernández-Jiménez A, Provis JL *et al.* (2007) Geopolymer technology: the current state of the art. *Journal of Materials Science* **42(9)**: 2917–2933.

Engelhardt G, Felsche J and Sieger P (1992) The hydrosodalite system Na6+x [SiAlO4]6(OH)x.cnt.nH, 2O, formation, phase composition, and de- and rehydration studied by ^{1}H, ^{23}Na, and ^{29}Si MAS-NMR spectroscopy in tandem with thermal analysis, X-ray diffraction, and IR spectroscopy. *Journal of the American Chemical Society* **114(4)**: 1173–1182.

Franus W, Wdowin M and Franus M (2014) Synthesis and characterization of zeolites prepared from industrial fly ash. *Environmental Monitoring and Assessment* **186(9)**: 5721–5729.

Gourav K and Venkatarama Reddy BV (2018) Bond development in burnt clay and fly ash-lime-gypsum brick masonry. *Journal of Materials in Civil Engineering* **30(9)**: 04018202.

Granizo ML and Blanco MT (1998) Alkaline activation of metakaolin an isothermal conduction calorimetry study. *Journal of Thermal Analysis and Calorimetry* **52(3)**: 957–965.

Habert G and Ouellet-Plamondon C (2016) Recent update on the environmental impact of geopolymers. *RILEM Technical Letters* **1**: 17–23.

Heath A, Maskell D, Walker P, Lawrence M and Fourie C (2012) Modern earth masonry: structural properties and structural design. *The Structural Engineer* **90(4)**: 38–44.

Heath A, Paine K and McManus M (2014) Minimising the global warming potential of clay based geopolymers. *Journal of Cleaner Production* **78**: 75–83.

HM Government (2013) *The Building Regulations 2010. Structure: Approved Document A*. NBS, Newcastle, UK.

Houben H and Guillaud H (1994) *Earth Construction: A Comprehensive Guide*. Practical Action Publishing, Rugby, UK.

Jagadish K (2007) *Building with Stabilized Mud*. I.K. International Publishing House Pvt. Ltd, New Delhi, India.

Kendrick E and Dann S (2004) Synthesis, properties and structure of ion exchanged hydrosodalite. *Journal of Solid State Chemistry* **177(4–5)**: 1513–1519.

Khalifa AZ, Cizer Ö, Pontikes Y *et al.* (2020) Advances in alkali-activation of clay minerals. *Cement and Concrete Research* **132**: 106050.

Kuenzel C, Li L, Vandeperre L, Boccaccini AR and Cheeseman CR (2014) Influence of sand on the mechanical properties of metakaolin geopolymers. *Construction and Building Materials* **66**: 442–446.

Lee WKW and van Deventer JSJ (2002) The effect of ionic contaminants on the early-age properties of alkali-activated fly ash-based cements. *Cement and Concrete Research* **32(4)**: 577–584.

Longhi MA, Zhang Z, Rodríguez ED, Kirchheim AP and Wang H (2019) Efflorescence of alkali-activated cements (geopolymers) and the impacts on material structures: a critical analysis. *Frontiers in Materials* **6**: 89, https://doi.org/10.3389/fmats.2019.00089.

Lucas S, Tognonvi MT, Gelet JL, Soro J and Rossignol S (2011) Interactions between silica sand and sodium silicate solution during consolidation process. *Journal of Non-Crystalline Solids* **357(4)**: 1310–1318.

Marsh A, Heath A, Patureau P, Evernden M and Walker P (2018) A mild conditions synthesis route to produce hydrosodalite from kaolinite, compatible with extrusion processing. *Microporous and Mesoporous Materials* **264**: 125–132.

Marsh A, Heath A, Patureau P, Evernden M and Walker P (2019) Influence of clay minerals and associated minerals in alkali activation of soils. *Construction and Building Materials* **229**: 116816, https://doi.org/10.1016/j.conbuildmat.2019.116816.

Maskell D, Heath A and Walker P (2014) Geopolymer stabilisation of unfired earth masonry units. In *Proceedings of the 14th International Conference on Non-Conventional Materials and Technologies for Sustainable Engineering* (Ghavami K, Barbosa NP, Bezerra A and Zhemchuzhnikov UT (eds)). Trans Tech Publications, Joao Pessoa, Brazil, pp. 175–185.

Mastali M, Kinnunen P, Dalvand A, Mohammadi Firouz R and Illikainen M (2018) Drying shrinkage in alkali-activated binders – a critical review. *Construction and Building Materials* **190**: 533–550.

McGregor F, Heath A, Fodde E and Shea A (2014) Conditions affecting the moisture buffering measurement performed on compressed earth blocks. *Building and Environment* **75**: 11–18.

McGregor F, Heath A, Maskell D, Fabbri A and Morel JC (2016) A review on the buffering capacity of earth building materials. *Proceedings of the Institution of Civil Engineers – Construction Materials* **169(5)**: 241–251, https://doi.org/10.1680/jcoma.15.00035.

Morel JC, Pkla A and Walker P (2007) Compressive strength testing of compressed earth blocks. *Construction and Building Materials* **21(2)**: 303–309.

Muñoz JF, Easton T and Dahmen J (2015) Using alkali-activated natural aluminosilicate minerals to produce compressed masonry construction materials. *Construction and Building Materials* **95**: 86–95.

Narayanaswamy AH, Walker P, Venkatarama Reddy BV, Heath A and Maskell D (2020) Mechanical and thermal properties, and comparative life-cycle impacts, of stabilised earth building products. *Construction and Building Materials* **243**: 118096.

NCEI (National Centers for Environmental Information) (2018) *Integrated Surface Database*. National Oceanic and Atmospheric Administration, Asheville, NC, USA.

Petrova N and Kirov GN (1995) Zeolitization of glasses: a calorimetric study. *Thermochimica Acta* **269–270**: 443–452.

Provis JL (2018) Alkali-activated materials. *Cement and Concrete Research* **114**: 40–48.

Provis JL, Duxson P and van Deventer JSJ (2010) The role of particle technology in developing sustainable construction materials. *Advanced Powder Technology* **21(1)**: 2–7.

Reddy B (2015) Design of a manual press for the production of compacted stabilized soil blocks. *Current Science* **109(9)**: 00113891.

Reddy BVV and Latha MS (2014) Influence of soil grading on the characteristics of cement stabilised soil compacts. *Materials and Structures* **47(10)**: 1633–1645.

Reeves GM, Sims I and Cripps JC (2006) *Clay Materials Used in Construction*. Geological Society, London, UK.

Rios S, Cristelo N, Viana Da Fonseca A and Ferreira C (2016) Structural performance of alkali-activated soil ash versus soil cement. *Journal of Materials in Civil Engineering* **28(2)**: 04015125.

Rovnaník P (2010) Effect of curing temperature on the development of hard structure of metakaolin-based geopolymer. *Construction and Building Materials* **24(7)**: 1176–1183.

Scrivener KL, John VM and Gartner EM (2018) Eco-efficient cements: potential economically viable solutions for a low-CO_2 cement-based materials industry. *Cement and Concrete Research* **114**: 2–26.

Silva RA, Soares E, Oliveira DV *et al.* (2015) Mechanical characterisation of dry-stack masonry made of CEBs stabilised

with alkaline activation. *Construction and Building Materials* **75**: 349–358.

Sivapullaiah PV, Sridharan A and Bhaskar Raju KV (2000) Role of amount and type of clay in the lime stabilization of soils. *Ground Improvement* **4(1)**: 37–45, https://doi.org/10.1680/grim.2000.4.1.37.

Walker PJ (1995) Strength, durability and shrinkage characteristics of cement stabilised soil blocks. *Cement and Concrete Composites* **17(4)**: 301–310.

Walker P and Stace T (1997) Properties of some cement stabilised compressed earth blocks and mortars. *Materials and Structures* **30(9)**: 545–551.

Walker P, Keable R, Martin J and Maniatidis V (2005) *Rammed Earth: Design and Construction Guidelines*. IHS BRE Press, Bracknell, UK.

Weng L and Sagoe-Crentsil K (2007) Dissolution processes, hydrolysis and condensation reactions during geopolymer synthesis: part I – low Si/Al ratio systems. *Journal of Materials Science* **42(9)**: 2997–3006.

Wijaya SW and Hardjito D (2016) Factors affecting the setting time of fly ash-based geopolymer. In *Properties and Application of Geopolymers* (Januarti JE and Antoni (eds)) Trans Tech Publications, Surabaya, Indonesia, pp. 90–97.

Zhang Z, Wang H, Provis JL *et al.* (2012) Quantitative kinetic and structural analysis of geopolymers. Part 1, the activation of metakaolin with sodium hydroxide. *Thermochimica Acta* **539(suppl. C)**: 23–33.

Zuhua Z, Xiao Y, Huajun Z and Yue C (2009) Role of water in the synthesis of calcined kaolin-based geopolymer. *Applied Clay Science* **43(2)**: 218–223.